Cell Reports

Resource

Proteomic and Metabolomic Characterization of a Mammalian Cellular Transition from Quiescence to Proliferation

Graphical Abstract

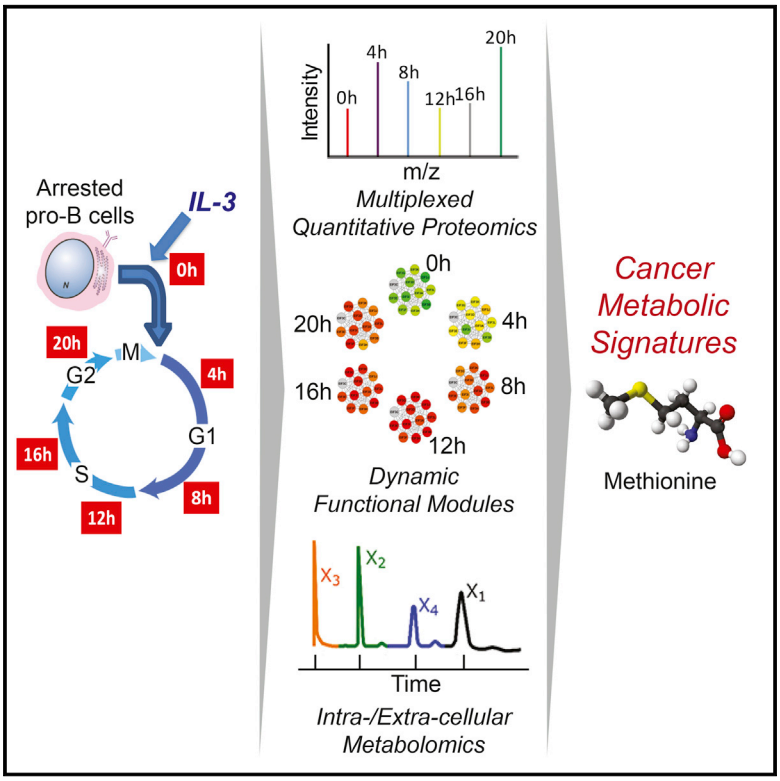

Highlights

- Proteomic and metabolomic temporal profiling from G0 to cell cycle in response to IL-3
- Global similarities in metabolic reprogramming with cancer cells
- Nucleotide metabolism is highly specialized during the proliferative transition
- Rapid consumption of methionine in G1 serving multiple functions

Authors

Ho-Joon Lee, Mark P. Jedrychowski, Arunachalam Vinayagam, ..., Steven P. Gygi, Lewis C. Cantley, Marc W. Kirschner

Correspondence

marc@hms.harvard.edu

In Brief

Lee et al. generate and integrate quantitative time-course proteomic and metabolomic profiling data to find that global metabolic reprogramming of an IL-3 activation resembles metabolic rewiring in cancer with high consumption of methionine in G1.

Accession Numbers

PXD006771

Lee et al., 2017, Cell Reports *20*, 721–736
July 18, 2017
http://dx.doi.org/10.1016/j.celrep.2017.06.074

CellPress

Cell Reports
Resource

Proteomic and Metabolomic Characterization of a Mammalian Cellular Transition from Quiescence to Proliferation

Ho-Joon Lee,[1,9,10] Mark P. Jedrychowski,[2,9] Arunachalam Vinayagam,[4,9] Ning Wu,[5] Ng Shyh-Chang,[6] Yanhui Hu,[4] Chua Min-Wen,[6] Jodene K. Moore,[1] John M. Asara,[7] Costas A. Lyssiotis,[3] Norbert Perrimon,[4] Steven P. Gygi,[2] Lewis C. Cantley,[8] and Marc W. Kirschner[1,11,*]

[1]Department of Systems Biology, Harvard Medical School, Boston, MA 02115, USA
[2]Department of Cell Biology, Harvard Medical School, Boston, MA 02115, USA
[3]Division of Gastroenterology, Department of Molecular and Integrative Physiology and Department of Internal Medicine, University of Michigan Medical School, Ann Arbor, MI 48109, USA
[4]Department of Genetics, Harvard Medical School, Boston, MA 02115, USA
[5]Center for Cancer and Cell Biology, Van Andel Research Institute, Grand Rapids, MI 49503, USA
[6]Stem Cell & Regenerative Biology, Genome Institute of Singapore, S138672 Singapore, Singapore
[7]Division of Signal Transduction, Department of Medicine, Beth Israel Deaconess Medical Center and Harvard Medical School, Boston, MA 02115, USA
[8]Meyer Cancer Center, Department of Medicine, Weill Cornell Medical College, New York, NY 10065, USA
[9]These authors contributed equally
[10]Present address: Department of Molecular and Integrative Physiology, University of Michigan Medical School, Ann Arbor, MI 48109, USA
[11]Lead Contact
*Correspondence: marc@hms.harvard.edu
http://dx.doi.org/10.1016/j.celrep.2017.06.074

SUMMARY

There exist similarities and differences in metabolism and physiology between normal proliferative cells and tumor cells. Once a cell enters the cell cycle, metabolic machinery is engaged to facilitate various processes. The kinetics and regulation of these metabolic changes have not been properly evaluated. To correlate the orchestration of these processes with the cell cycle, we analyzed the transition from quiescence to proliferation of a non-malignant murine pro-B lymphocyte cell line in response to IL-3. Using multiplex mass-spectrometry-based proteomics, we show that the transition to proliferation shares features generally attributed to cancer cells: upregulation of glycolysis, lipid metabolism, amino-acid synthesis, and nucleotide synthesis and down-regulation of oxidative phosphorylation and the urea cycle. Furthermore, metabolomic profiling of this transition reveals similarities to cancer-related metabolic pathways. In particular, we find that methionine is consumed at a higher rate than that of other essential amino acids, with a potential link to maintenance of the epigenome.

INTRODUCTION

In addition to nutrients, mammalian cells require extracellular growth factors to grow and proliferate (Conlon and Raff, 1999; Pardee, 1989; Sherr, 1994; Zetterberg, 1990). Absent such factors, many types of cells survive in a quiescent, or G0, state. Re-introduction of growth factors will drive these cells into the cell cycle. This process, which leads to a change of cell state, has intrigued researchers from the early days of mammalian cell culture. Numerous experiments have been performed with serum deprivation/reintroduction protocols to study the kinetics of how cells in the G0 state re-enter the cell cycle (Planas-Silva and Weinberg, 1997; Zetterberg et al., 1995). In recent proteomic studies, T cell activation was used to characterize, specifically, nuclear and mitochondrial changes as cells transitioned from G0 to G1 (Orr et al., 2012; Ron-Harel et al., 2016). While these experiments identified several cellular behaviors, we believed that a more global search of protein expression could lead to more complete understanding of this important transition. Today, many of the obstacles to proteome-wide quantitative mass spectrometry (MS) have been overcome, but the issues of depth of proteomic coverage still remain, with some classes of abundant proteins easily measured and other rarer proteins like receptors, secreted signaling molecules, and transcription factors under-sampled. However, for many protein families and pathways, the coverage is good enough to be confident about making solid generalizations. This is particularly true for the very abundant metabolic enzymes, which can provide comprehensive insights into the state of cellular metabolism.

We have characterized the cytokine-mediated transition of the pro-B lymphocyte cell line, FL5.12 (McKearn et al., 1985), from a quiescent state to a proliferative state at the proteomic level. FL5.12 cells are exclusively dependent on interleukin (IL)-3 for cell growth and proliferation and can be synchronized in the G0 state by IL-3 removal and induced to proliferate by adding IL-3. As such, they provide a better controlled experiment relative to the addition and removal of the complex mixture of growth factors

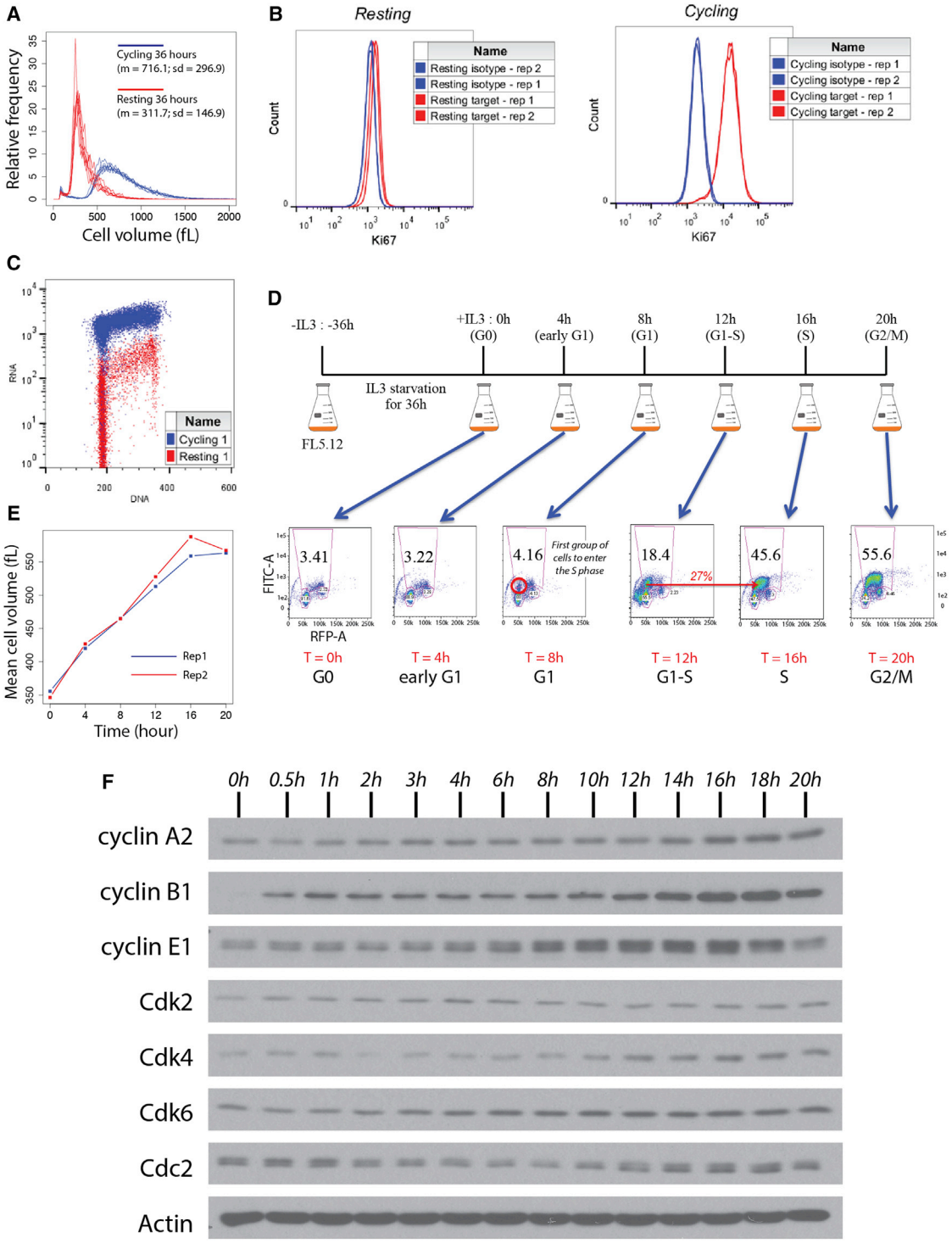

Figure 1. The Murine Pro-B Lymphocyte Cell Line, FL5.12, Exclusively Depends on IL-3 for Growth and Proliferation

We synchronized cells at a quiescence/resting state or G0 by growing in media without IL-3 for 36 hr and then released them from G0 into the cell cycle by re-growing them in the presence of IL-3.

(A) Cell-size distributions of cycling cells in the presence of IL-3 and resting (or G0) cells in the absence of IL-3 for 36 hr, with seven replicates measured using a Coulter counter.

(B) The proliferation marker, Ki-67, shows that FL5.12 cells in G0 do not express Ki-67 and that the cycling cells sampled at 36 hr express Ki-67.

(legend continued on next page)

found in serum. We used an FL5.12 cell line that expresses Bcl-2 to prevent apoptosis when IL-3 is removed for several days (Nuñez et al., 1990). For analysis, we have used a versatile multiplex method for quantitative MS that uses tandem isobaric mass tags that can simultaneously determine the ratio of a given protein in several samples (Singh et al., 2014; Thompson et al., 2003; Ting et al., 2011). We found that the predominant proteomic changes during transition through the cell cycle were metabolic. We bolstered the proteomic studies with mass-spectrometry-based metabolomics analyses. Collectively, these revealed that intermediary metabolism in pro-B cell proliferation bears strong similarity to cancer metabolism, including major changes in translation machinery and nucleotide and methionine pathways.

RESULTS

Features of Quiescence and Cell-Cycle Entry

Cells in the G0 phase of the cell cycle are defined by a lack of proliferation (marked by low Ki-67 and high Cdkn1b/p27 expression), reduced cell size, and active autophagy. Reduced metabolic activity or flux rates are not always a hallmark of the quiescent state (Lemons et al., 2010). IL-3-deprived FL5.12 cells meet several of the qualifications for the G0 state. After 36 hr of IL-3 depletion, FL5.12 cells cease dividing, the mean cell size decreases, and there is a decrease in size variation (Figures 1A and 1D). Ki-67 antibody staining declines 35-fold, as assayed by flow cytometry (Figure 1B). There is also a decrease in RNA content, as measured by acridine orange (AO) staining, another reported characteristic of the G0 state (Figure 1C) (London and McKearn, 1987).

When stimulated by IL-3, FL5.12 cells resume growth and proliferate. We characterized the kinetics of the quiescent-proliferative transition by measuring G1 length and entry into S phase by bromodeoxyuridine (BrdU)-7AAD (7-Aminoactinomycin D) incorporation and flow cytometry, cell volume by Coulter counter, and the expression of various cell-cycle markers by western blot. S phase begins at 8–12 hr for >10% of cells (Figure 1D). Cell size increases from 350 fL to ~550 fL as cells go through the first cell cycle (Figure 1E). There is asynchrony in the cell-cycle distribution with time, and this is reflected in the broadening of the size distributions. We profiled cyclins and cyclin-dependent kinases (Figure 1F) (Malumbres and Barbacid, 2005; Murray, 2004; Sherr and Roberts, 2004). Cyclin E begins to increase at 8 hr, consistent with the BrdU measurements, thus denoting the G1/S transition. Cyclin A, cyclin B, and Cdk1 increased at 16–20 hr, characteristic of the G2-M phases.

Dynamics of Protein Expression

Using 6-plex tandem mass tags (TMTs), we measured the relative levels of different proteins at different times during the transition from G0 into the cell cycle (Experimental Procedures) (Ting et al., 2011). In biological duplicate experiments, we quantitated 43,000 unique peptides corresponding to 6,700 unique proteins; >4,700 were common to both experiments (Figure S1A). The relative expression of each protein was defined to be the average profile of all corresponding peptides from each experiment. Each temporal profile was normalized by its mean value for the purposes of comparison and visualization. 2,666 proteins show well-correlated profiles between the duplicates; these reproducible proteins were the focus for subsequent analysis (Pearson correlation coefficient, >0.5; Data S1).

Unsupervised hierarchical clustering of the 2,666 protein abundance changes, using the Euclidean distance as a similarity metric after standardization, showed that duplicate experiments cluster together at each time point and also recaptured the temporal order, suggesting overall gradual changes of protein expression over time (Figure 2A). The global expression pattern yields two different temporal clusters corresponding to a transition phase from G0 into G1 (0 hr and 4 hr) and another clear transition from mid-G1 onward into S phase and mitosis (8 hr to 20 hr). There are two main groups of proteins that have opposing expression patterns, where one group is upregulated in G0/G1 and downregulated in S/M/G2 and the other main group exhibits the opposite pattern. For subsequent analysis, we averaged the expression profiles from the duplicate experiments and performed principal-component analysis (PCA) to obtain a different global view of the data. The first two principal components (PCs) explained 86.9% of the total variation (Figure S1B). The first two time points (G0/G1 transition) were clearly distinguished from the remaining time points (Figure S1B), consistent with the hierarchical clustering analysis. Moreover, the two PCs identified several individual proteins whose expression variations make a major contribution to each PC (Figure S1B).

To identify individual dynamic proteins, we calculated the maximum fold change (MFC), defined as the ratio of the maximum level to the minimum level for a given expression profile. The mean value of MFCs of 2,666 protein profiles is ~1.53, and the median is ~1.38. There are 240 proteins whose MFCs are greater than 2. The top two proteins, Nek6 and Phlda1, have MFCs of approximately 29 and 18, respectively. Nek6 is serine/threonine-protein kinase or NimA-related kinase, which plays an important role in mitotic cell-cycle progression and is also a cancer therapeutic target (Jeon et al., 2010; Meirelles et al., 2014; Nassirpour et al., 2010). Phlda1, pleckstrin homology-like domain family A member 1, is involved in the apoptotic response (Park et al., 1996; Toyoshima et al., 2004). Nek6 and Phlda1 were increased 15- and 13-fold, respectively, from time, t, = 0 hr to t = 4 hr (the highest top two), suggesting that

(C) An acridine orange (AO) assay distinguishes the resting G0 population from the cycling population by the RNA content. The IL-3-deprived G0 cells have lower RNA content than the cycling population.
(D) A 30-min incubation with BrdU shows how the FL5.12 cells progress into the cell cycle from G0 upon IL-3 stimulation. Samples were collected every 4 hr over the 20 hr of this study. The G1/S transition occurred between 12 hr and 16 hr for the majority of cells.
(E) Cell size changes after IL-3 stimulation in duplicates.
(F) Western blotting analysis of seven cell cycle markers: cyclins A2, B1, and E1; Cdk2, -4, and -6; and Cdc2 (a.k.a. Cdk1). Actin was used as a control. The G1/S transition can be seen at around 10 hr from cyclin E; G2/M phases from cyclins A2/B1 and Cdc2.
rep, replication.

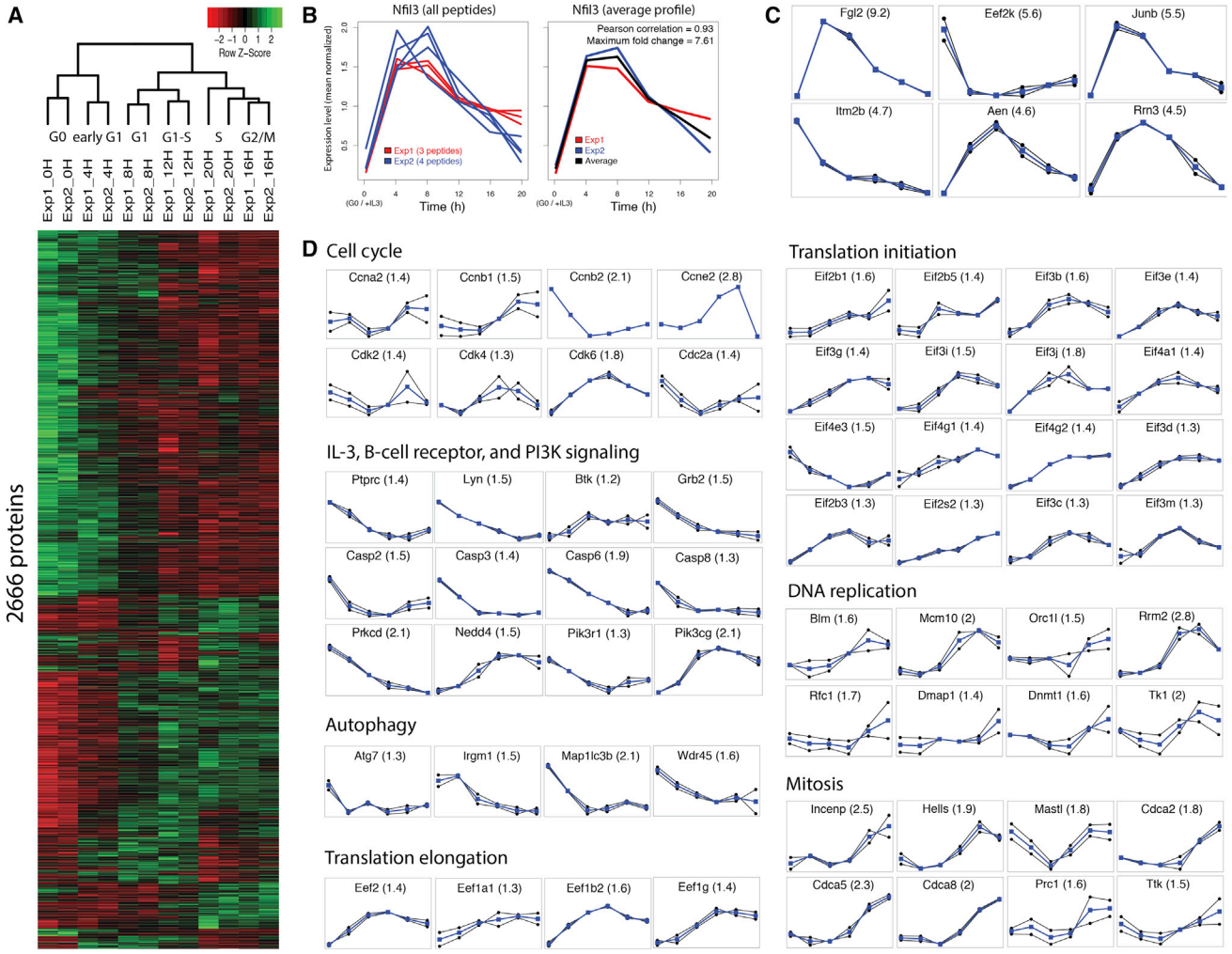

Figure 2. Proteomics Data of Temporal Expression and Highly Confident Individual Proteins

The data are based on Pearson correlation coefficients (rs) between all pairs of peptides from the duplicate experiments.

(A) Unsupervised hierarchical clustering of 2,666 proteins whose expression profiles from duplicate experiments have rs > 0.5.

(B) A representative expression profile from our TMT data. The top second protein from (A), Nfil3, is shown. It is a transcription factor that positively responds to IL-3. The left panel shows profiles of all peptides detected from our duplicate TMT experiments. The right panel shows their averaged profiles for the protein itself. Upon the IL-3 activation, the expression level of Nfil3 was highly upregulated as expected. We used averaged profiles for individual proteins in the subsequent main text.

(C) Temporal expression profiles of the six highly confident proteins with an MFC > 4.

(D) Manually selected confident protein profiles for seven cellular processes.

both mitosis and apoptosis immediately respond to the IL-3 activation for the transition from G0 into the cell cycle.

We identified 16 highly confident proteins where all pairs of peptides have Pearson correlation coefficients greater than 0.8 and that suggest that the proteomic data mirror expected cellular responses. Among these are seven proteins with an MFC > 4: Fgl2 (or Fibroleukin), Nfil3, Eef2k, Junb, Itm2b, Aen, and Rrn3. Fgl2, Nfil3, Eef2k, Junb, and Rrn3 were among the top targets based on PCA and MFC, as described earlier. The expression profile of Nfil3, a transcription factor limited to T cells and related cells, shown in Figure 2B, demonstrates that the data from the duplicate experiments can be very reliable on the measured peptide level and that the upregulation in G1 is as expected for a response to the IL-3 activation. Fgl2, with the highest MFC, 9.2, is a 432-amino-acid transmembrane regulator in both innate and adaptive immunity. It has a role in the negative regulation of regulatory T (Treg) cell proliferation and the positive regulation of B cell apoptosis (Shalev et al., 2008). Our data confirm that it should be downregulated in G0, reflecting the suppression of apoptosis due to Bcl-2, and highly upregulated in response to IL-3, peaking at 4 hr of early G1 (Figure 2C). Eef2k is a kinase that is involved in translational inhibition by suppressing a translation elongation factor, Eef2. Junb, which increases about 6-fold on going from G0 to G1, is a transcription factor that is upregulated in response to growth factors; Itm2b is a broadly expressed membrane protein of unknown function; it

continually decreases ~4.5-fold from G0 to G2/M. Aen is an exonuclease downstream of p53 with a role in amplifying apoptotic signals; its abundance is the lowest in G0, increases up to ~4.5-fold in mid-G1 and then decreases in the proliferative state of S/G2/M. Rrn3 is an RNA polymerase I (Pol I)-specific transcription initiation factor for rDNA. The interaction of Rrn3 and Pol I is essential for rDNA transcription, and they dissociate upon transcription (Hirschler-Laszkiewicz et al., 2003). Its upregulation by ~4.4-fold between G0 and G1 is consistent with a growth signal by IL-3 or the increasing abundance of ribosomal proteins. The following downregulation suggests its dissociation from Pol I upon rDNA transcription as the growth signal diminishes. In Figure 2D, we illustrate 60 proteins that also give highly confident patterns, but with smaller MFC, and that illustrate the regulation of several cellular processes on entering a proliferative phase: cell cycle, IL-3, B cell receptor, and phosphatidylinositol 3-kinase (PI3K) signaling, autophagy, translation initiation, translation elongation, DNA replication, and mitosis.

To obtain more global functional insight, we performed functional enrichment analysis by the hypergeometric test using Gene Ontology (GO) terms (Experimental Procedures). The most significant terms with a p value < 0.001 include nucleolus, ribosome, mitochondrion, structural constituents of ribosomes, ATP binding, translation initiation factor activity, translation, and rRNA processing, which are mostly upregulated on entry to the cell cycle (Figure S2). This suggests that translation/protein synthesis-related proteins play important roles during the proliferative transition of quiescent FL5.12 cells in response to IL-3, in agreement with a previous study on T cell activation entering the first cell cycle (Orr et al., 2012).

Dynamics of Protein Modules

We can produce a narrative for one protein at a time that is useful in validating our general study of physiological regulation on entering the cell cycle. However, such tedious narrative building fails when dealing with poorly characterized proteins or with proteins where there was no clear expectation of behavior. To consider the problem in a more objective fashion, we analyzed the proteomic results in terms of functionally related protein groups or modules, which includes, but is not limited to, physical protein complexes. First, based on our previous efforts in other species (Vinayagam et al., 2013), we built a large repository of mouse protein modules by systematically compiling known and predicted modules (Experimental Procedures). We then applied the COMPLEAT tool (Vinayagam et al., 2013) to analyze our proteomic TMT data and to generate temporal expression profiles of modules (Experimental Procedures). We identified significantly enriched modules based on module scores and p values (Experimental Procedures). An example of a module, the condensin complex, and its abundance profile are shown in Figure 3A.

We prioritized dynamically regulated modules using multiple filtering criteria (Figures 3B–3E; Experimental Procedures). This yielded a final list of 821 dynamic modules, with 311 of them literature supported (Figure 3E; Data S1). We found that 10%–15% of all protein modules from the literature are dynamic during the transition from G0 to the first cell cycle. Unsupervised hierarchical clustering of the 311 literature-supported modules clearly distinguishes the G0/G1 transition from the cell cycle (Figure S3A). Thus, the behavior of these literature-supported dynamic modules show behavior consistent with proteomic changes discussed earlier (Figure 2A).

To search for other characteristic dynamic features during the cell cycle, we identified modules whose scores peaked at each time point. The G0 state had the highest fraction of 32% (Figure 3F). The peak modules from 4 hr to 20 hr in Figure 3F include physical complexes functioning in: IL-3 signaling (4 hr), transcription initiation (8 hr), ribosome biogenesis (12 hr), DNA replication (16 hr), and mitosis (20 hr). The module at 0 hr, the citrate cycle, is a group of functionally related enzymes to which we pay particular attention in the next section. As a means to further functionally support the identified modules, we also built a global functional map of the 311 dynamic modules by organizing them using GO enrichment (Figure S3B). From this map, we could manually identify 77 unique modules as confidence builders, functioning in 15 biological processes from which we can expect certain expression patterns (Figure S3B).

The Cell-Cycle Entry from G0 Shares Several of the Hallmarks of Cancer Metabolism

From our global functional map of protein modules, we paid particular attention to the TriCarboxylicAcid cycle (TCA cycle) because all four modules show significant coherence of expression, including the module of citrate cycle (Figure 3F), also referred to as second carbon oxidation (MC2490). Cancer cells, a prototype for proliferative cells (Vander Heiden et al., 2009), repress mitochondrial metabolism in favor of ATP generation through glycolysis. The observed downregulation of four TCA modules suggests that FL5.12 cells behave similarly as they exit the resting state and enter the cell cycle. This observation drove us to look at other metabolic pathways related to cancer as well as individual metabolic enzymes. We examined closely eight metabolic pathways: the TCA cycle, glycolysis, de novo pyrimidine biosynthesis, de novo purine biosynthesis, pyrimidine salvage, purine degradation, lipid synthesis, and the urea cycle (Figures 4, 5, and S4A–S4H). The urea cycle was included in this list of biosynthetic pathways, because it has ties to nitrogen and nucleotide metabolism and was shown to be downregulated in some cancer cells (Feun et al., 2008; Phillips et al., 2013).

We detected all the TCA cycle enzymes, as well as the pyruvate dehydrogenase (PDH) complex (Pdhb, Pdha1, and Pdhx; see Figure 4A). Collectively, their temporal profiles show consistent and statistically significant downregulation during the proliferative transition ($p < 0.004$; Figure 4B; Table S1). Note that Pdk1/2/3, the kinase family that inhibits the PDH complex in the entry to the TCA cycle, is upregulated (Peters, 2003). The downregulation of the TCA cycle is also supported by an overall downregulation of component proteins of the electron transport chain (ETC) complexes (Figure S4I). In contrast, the behavior in glycolysis is just the opposite (Figures 4C and S4B). Txnip, the inhibitor of glucose transport, is downregulated, and Slc2a1 (Glut1), the glucose transporter, is upregulated during the G0/G1 transition. This was previously observed (Wu et al., 2013) and confirmed by western blotting in our study (Figure 4C). The

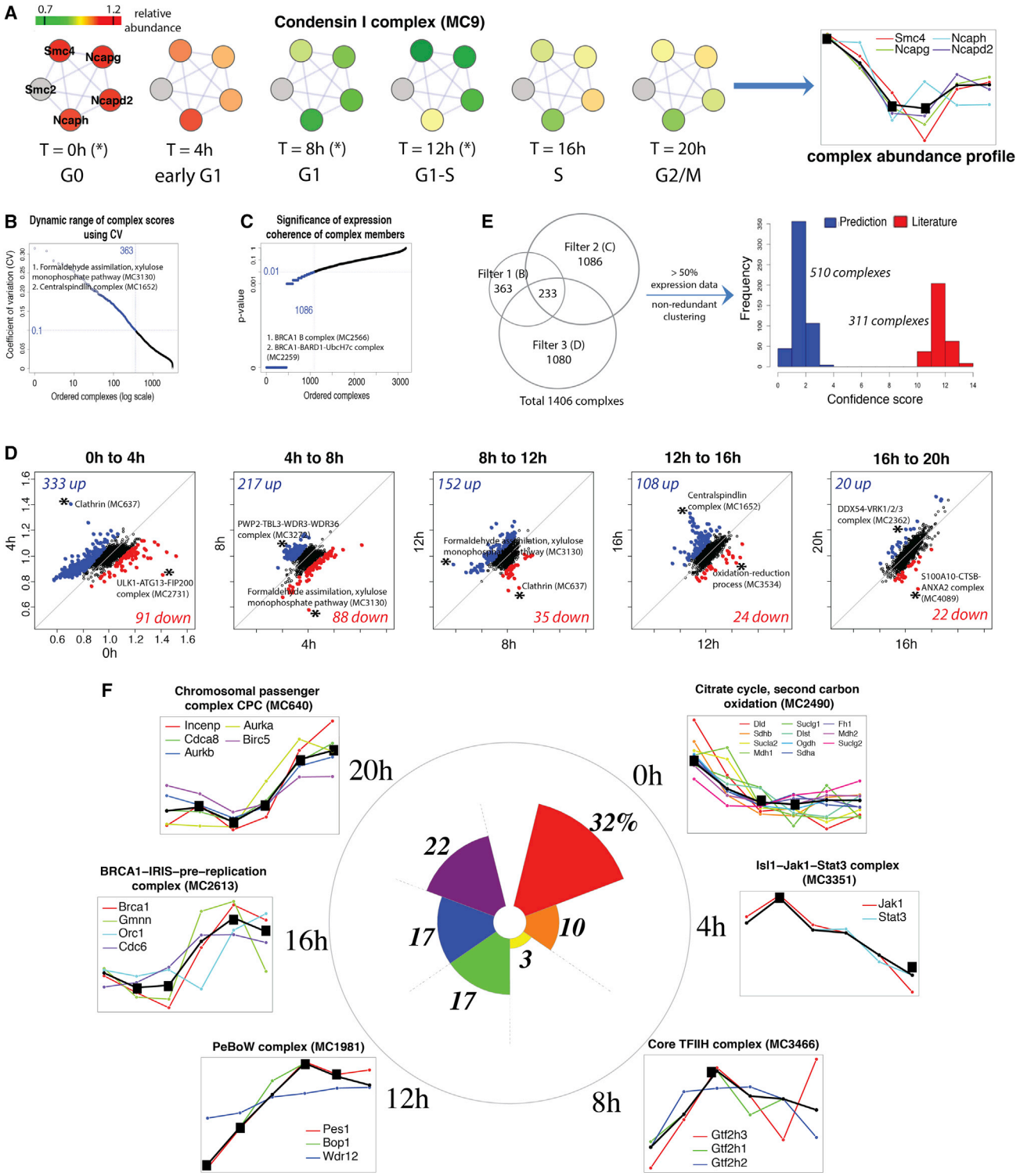

Figure 3. Analysis of Multi-protein Modules/Complexes

(A) An example complex, condensin I complex (MC9), is shown to illustrate how the complex abundance profile is derived. Condensin I complex is composed of five proteins, among which Smc2 (gray) was not detected in our TMT experiments. The relative abundance levels of the component proteins from the TMT data are color coded at each time point. Then, the COMPLEAT tool generates the complex abundance profile (in black). The x axis indicates the six time points, and the y axis indicates mean-normalized abundance levels in an arbitrary unit. The black square means that a module score is enriched or statistically significant at a given time point with a $p < 0.01$.

(legend continued on next page)

activation of glucose uptake is among the best characterized features of cancer metabolism (Bauer et al., 2004; Ying et al., 2012; Yun et al., 2009). Moreover, all the ATP-generating and rate-limiting enzymes in glycolysis—Hk2/3, Pfkl, Pfkm, Pfkp, and Pkm2—and Eno3 are also upregulated upon the transition into the cell cycle, suggesting that the activation of glycolysis in this context is a highly coordinated process.

All enzymes in the pyrimidine and purine de novo biosynthetic pathways (Figures S4C and S4D), are upregulated during G0/G1 transition, as expected for cell growth and proliferation. Some anabolic enzymes in nucleotide biosynthesis—including rate-limiting enzymes such as Cad, Gart, Adsl, Adss, and Impdh1/2—increase in G1 and reach maximal levels after the S phase. The upregulation of each enzyme group is statistically significant ($p < 0.04$; Table S1). In the pyrimidine salvage pathway (Figure S4E), Uprt and Uck2, which convert uracil, uridine, and cytidine to UMP and CMP, are also upregulated during the G1 phase and then downregulated thereafter. On the other hand, Cmpk1, Entpd3, and Nme3, which regulate uridine phosphate levels, are downregulated. In the purine degradation pathway (Figure S4F), most enzymes are downregulated. The coordinated up- and downregulation of the biosynthesis and salvage pathways, respectively, illustrate how the cells regulate the generation of new nucleotides for genome duplication. Acetyl-CoA (coenzyme A) carboxylase 1 (Acaca), the rate-limiting enzyme in fatty acid synthesis that converts acetyl-CoA to malonyl-CoA; fatty acid synthase (Fasn); and HMG-CoA synthase (Hmgcs1) are upregulated in the G1 phase and would seem to accelerate lipid biosynthesis, presumably to support biomass generation. In addition, we find that a cytoplasmic fatty acid binding protein, Fabp5, is upregulated in the proliferative state of G1 to S (Figure S4G). Fabp5 has been shown to be highly upregulated in human breast cancers and is a prognostic marker and a potential therapeutic target (Levi et al., 2013; Liu et al., 2011).

The canonical urea cycle consists of five enzymes, but not all five enzymes are necessarily expressed in all cell or tissue types (Morris, 2002). We detected three enzymes: carbamoyl phosphate synthase 1 (Cps1), argininosuccinate synthase (Ass1), and argininosuccinate lyase (Asl), which are all downregulated upon IL-3 activation (Figure S4H). In particular, the rate-limiting enzyme Cps1 exhibits a dramatic 4.8-fold decrease in its abundance during the first 4 hr of the G0/G1 transition. The downregulation of the urea cycle presumably favors the use of nitrogen for biosynthetic purposes of cell growth over the excretion of urea. The downregulation of the three enzymes as a group is statistically significant ($p < 0.02$; Table S1).

Correlation of Metabolite Levels with Enzymes

We were interested in whether the very clear changes in metabolic enzymes were reflected in their metabolites. Using a general metabolomics platform (Yuan et al., 2012), we detected 291 metabolites at the six time points in biological triplicates and obtained a filtered list of 155 metabolites for subsequent analysis (Experimental Procedures; Data S1). Unsupervised hierarchical clustering revealed that the data are reproducible and that the metabolomic profiles are similar between neighboring time points (Figures S5A and S5B). However, unlike the global proteomic changes that show significant changes at the G0/G1 transition (Figure 2A), the global metabolomic changes are seen as cells begin to enter S phase (t = 12 hr onward). 106 metabolites show coefficients of variation (CVs) less than 0.4 at all time points, which we consider as confidently measured.

In order to make a comparison between protein enzymes and metabolites, we mapped all confidently measured metabolites to the eight metabolic pathways discussed earlier. The vast majority of enzymes show consistent patterns, but this is much less true for their metabolites. The fluctuation of metabolites is also greater than that of enzyme levels (MFC = 7.2 versus 4.3, respectively). Enzymes that are consistently downregulated in the TCA cycle showed variable metabolite patterns (Figures 4A and 4B). Some metabolites such as citrate, isocitrate, alpha-ketoglutarate, fumarate, and malate are upregulated during the G0-G1 transition. In glycolysis (Figure S4B), the proteomics data showed that the abundance of the glucose transporter (Glut1) increases and that the profiles of rate-limiting enzymes such as Hk2/3, Pfkl/m/p, and Pkm2 are suggestive of increased glycolytic flux. This is not altogether surprising, as we would expect to have seen greater correlations of enzyme level with metabolite flux, since enzymes would increase the rate of the reactions.

A closer correlation between enzymes and their metabolites can be found in pathways other than sugar metabolism. In the de novo pyrimidine biosynthesis pathway (Figure S4C), the enzymes are upregulated, presumably in response to the increased demand for nucleotides during cell growth and proliferation. The final product, UMP, is upregulated as the cells pass through the cell cycle, while dihydroorotate is consumed as expected for pyrimidine synthesis during cell growth. Similar trends are observed for the purine de novo pathway (Figure S4D). The 12 enzymes and the end products, AMP and GMP, are consistently upregulated after entry into the cell cycle. In the pyrimidine salvage pathway (Figure S4E), the anabolic enzymes, Uprt and Uck2, are upregulated during G1, while the catabolic enzymes, Cmpk1, Nme3, and Entpd3, are downregulated, as expected.

(B) A distribution of coefficient of variations (CVs) of temporal profiles of the 3,177 significant modules. We chose a threshold of 0.1 to obtain 363 dynamic modules. The top two modules, formaldehyde assimilation, xylulose monophosphate pathway (MC3130) and centralspindlin complex (MC1652), are highlighted.
(C) A distribution of p values for expression coherence of component proteins in 3,177 significant modules. We chose a threshold of 0.01 to obtain 1,086 dynamic modules. The top two modules, BRCA1 B complex (MC2566) and BRCA1-BARD1-UbcH7c complex (MC2259), are highlighted.
(D) Scatterplots of fold changes of module scores at the adjacent time steps for 3,177 significant modules. Based on the histogram of all fold changes, thresholds of 1.1 and 0.9 are chosen for upregulation (in blue) and downregulation (in red), respectively. The numbers of up-/downregulated modules are shown, along with the top up-/downregulated modules (indicated by asterisks).
(E) The final list of 821 dynamic modules is obtained from the union of the three sets of dynamic modules from (B), (C), and (D). We retained only those modules in which more than 50% of whose their component proteins have the TMT expression data, and then we clustered to generate non-redundant modules. We focused on the 311 literature-supported modules (confidence score > 10) in this study.
(F) The sector plot represents the fraction of modules whose scores become the maximum at each time point. Example module profiles are shown at all time points.

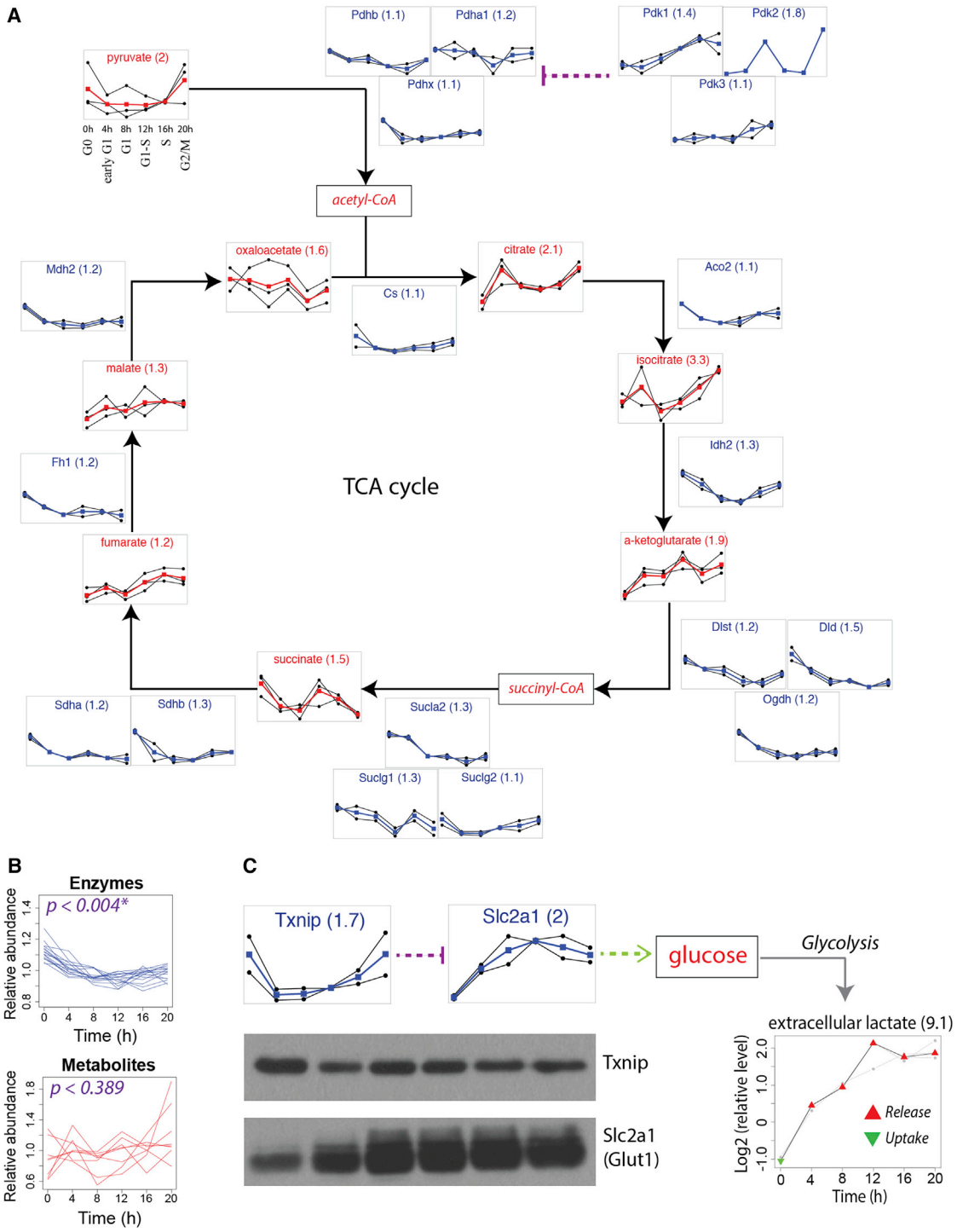

Figure 4. Downregulation of the TCA Cycle and Upregulation of Glycolysis

(A) Schematic representation of the TCA cycle with temporal profiles of enzymes and metabolites detected. Enzymes are indicated in blue (average), with duplicates in black, and metabolites are indicated in red (average), with triplicates in black. The x axis indicates the six time points, and the y axis indicates mean-normalized abundance levels in an arbitrary unit. The number in the parentheses next to each molecule name shows the maximum fold change (MFC) over the 20 hr.

(B) The average profiles of all 16 enzymes and metabolites in the TCA cycle. The enzyme profiles show a statistically significant coherent downregulation ($p < 0.004$), unlike the metabolite profiles ($p < 0.389$).

(C) Upregulation of glycolysis was observed through downregulation of Txnip and upregulation of Slc2a1 from the proteomics data and high release of lactate from the metabolomics data. Western blotting shows consistent expression patterns of Txnip and Slc2a1.

Correspondingly, the upstream metabolites, uracil, uridine, and cytidine, are downregulated, and the downstream metabolites, UMP, UDP, UTP, CMP, CDP, and CTP, are upregulated over time. In the purine degradation pathway (Figure S4F), the enzymes are downregulated, and the metabolites show a sharp decrease in their abundance during the G0/G1 transition. This implies that the degradation pathway is not activated, favoring purine synthesis for cell growth. The eight metabolites detected in this pathway are downregulated in a statistically significant fashion ($p < 0.003$; Table S1). In the urea cycle (Figure S4H), carbamoyl phosphate levels exhibit a large gradual decrease (MFC = 5.4), presumably reflecting the major downregulation of Cps1. This may also be related to increased pyrimidine synthesis, which consumes carbamoyl phosphate. We also observe corresponding decreases of ornithine and urea, possibly reflecting the use of free nitrogen for biosynthetic purposes.

Despite some expected correlations, the changes in the relative abundance of enzymes and metabolites are not easily explained. To search for explanations, we looked for correlations between enzymes and metabolites in each pathway. We first obtained average enzyme and metabolite time profiles (Figure 5A). The TCA cycle, glycolysis, and lipid synthesis showed no obvious correlations between enzyme and the corresponding metabolite levels, while other pathways show either positive or negative correlations. To better quantify these relationships, we calculated absolute Pearson correlation coefficients for all pairs between enzyme abundance profiles and metabolite abundance profiles and their mean value in each of the seven metabolic pathways, excluding lipid synthesis, in which only one metabolite (citrate) was measured. For each pathway, we performed a statistical significance test for the mean value by random sampling of enzymes and metabolites (Experimental Procedures). The correlations between enzyme and metabolite profiles are, overall, better than expected by chance ($p < 0.09$), except for the TCA cycle and glycolysis ($p > 0.4$) (Figure 5A). This was expected due to large variation in metabolite abundance considered earlier. The most likely explanation is that metabolites in these pathways are also acted on by enzymes in other pathways, which have their own dynamics (Ward and Thompson, 2012). In contrast, metabolites in nucleotide metabolism are more restricted to their specific pathways and, as such, exhibit correlations.

We also looked for cross correlations between enzyme profiles in one pathway and metabolite profiles in another pathway to understand inter-relationships. This modular cross-correlation analysis generated an asymmetric correlation matrix of the eight pathways (Figure 5B). The enzymes in the TCA were strongly correlated to the metabolites in the urea cycle, but those enzymes were negatively correlated with metabolites in glycolysis and TCA. The enzymes in those cycles were negatively correlated with TCA metabolites and glycolysis metabolites. The metabolites in glycolysis and the TCA cycle are positively correlated with the enzymes in the pyrimidine and purine de novo pathways, while they are negatively correlated with the enzymes in the purine degradation and the pyrimidine salvage pathway. For a further global insight, we paid particular attention to those cross-correlations that are better than either of the two within-pathway correlations. As shown in Figure 5C, the enzyme profiles in glycolysis have higher correlations with the metabolite profiles in all the other six pathways than those in glycolysis itself. This, again, supports the fact that glycolytic intermediates are used as precursors for several other metabolic pathways, among which are nucleotide and amino-acid biosynthetic pathways. On the other hand, the measured enzymes in nucleotide metabolism and the urea cycle do not show such high cross-correlations, implying that those enzymes are specific to their pathways. We conclude that metabolite dynamics show more complex patterns than enzyme dynamics and that nucleotide metabolism is a more specialized process than others showing correlated dynamics between enzymes and metabolites.

Extracellular Metabolite Profiling Underscores Proliferative Metabolic Changes

Another very useful perspective of metabolic changes is revealed in how metabolites are consumed from and released into the growth medium. The metabolite levels in the control fresh media were used as a reference for all time points. Unsupervised hierarchical clustering again revealed that the data are reproducible and that the neighboring time points have similar profiles, except for t = 0 hr (Figure S5C). It is reasonable that the abundance levels of extracellular metabolites in the media at t = 0 hr, which is the G0 state after the 36-hr IL-3 deprivation, are similar to those at t = 16 hr and 20 hr rather than t = 4 hr, in accordance with longer consumption of/exposure to the extracellular media. By dividing by the control media metabolite levels, we obtained a final list of 173 normalized metabolite levels for all time points (Figure S5D; Data 1). As a measure of the dynamic range of abundance levels, we calculated the MFC as described earlier. There are 44 metabolites with an MFC greater than 4, among which 11 metabolites have an MFC greater than 10. The top two dynamic metabolites are lysine (Lys) and methionine (Met), which showed an MFC > 110 and an MFC > 50, respectively. Both metabolites were consumed from the media by the cells, especially at the G0 and S/G2/M phases. Three other amino acids—phenylalanine (Phe), valine (Val), and tryptophan (Trp)—show a similar pattern of rapid consumption over time, meaning that they were depleted from the media as the cells entered the S phase.

Extracellular levels of pyruvate and lactate increased during the first cell cycle (Figure 6A), which provides clear support for upregulation of glycolysis during the proliferative transition and functionally validating the proteomics data discussed earlier (Figure 4B). Interestingly, we also observed that lactate in the media was consumed by the cells in G0. This likely reflects an effort by these cells to obtain and utilize non-glucose carbon sources, since glucose uptake is downregulated through Txnip-dependent repression of glucose transporter expression in G0, as discussed earlier.

Amino-Acid Consumption as a Function of the Cell Cycle

The proliferative transition accompanies the upregulation of translation and ribosome biogenesis (Figures 2D, 3F, S2, and S3B), suggesting correlated changes in amino-acid uptake, biosynthesis, and utilization. To quantify amino-acid consumption, we converted the normalized relative values into absolute concentrations at each time point based on the media

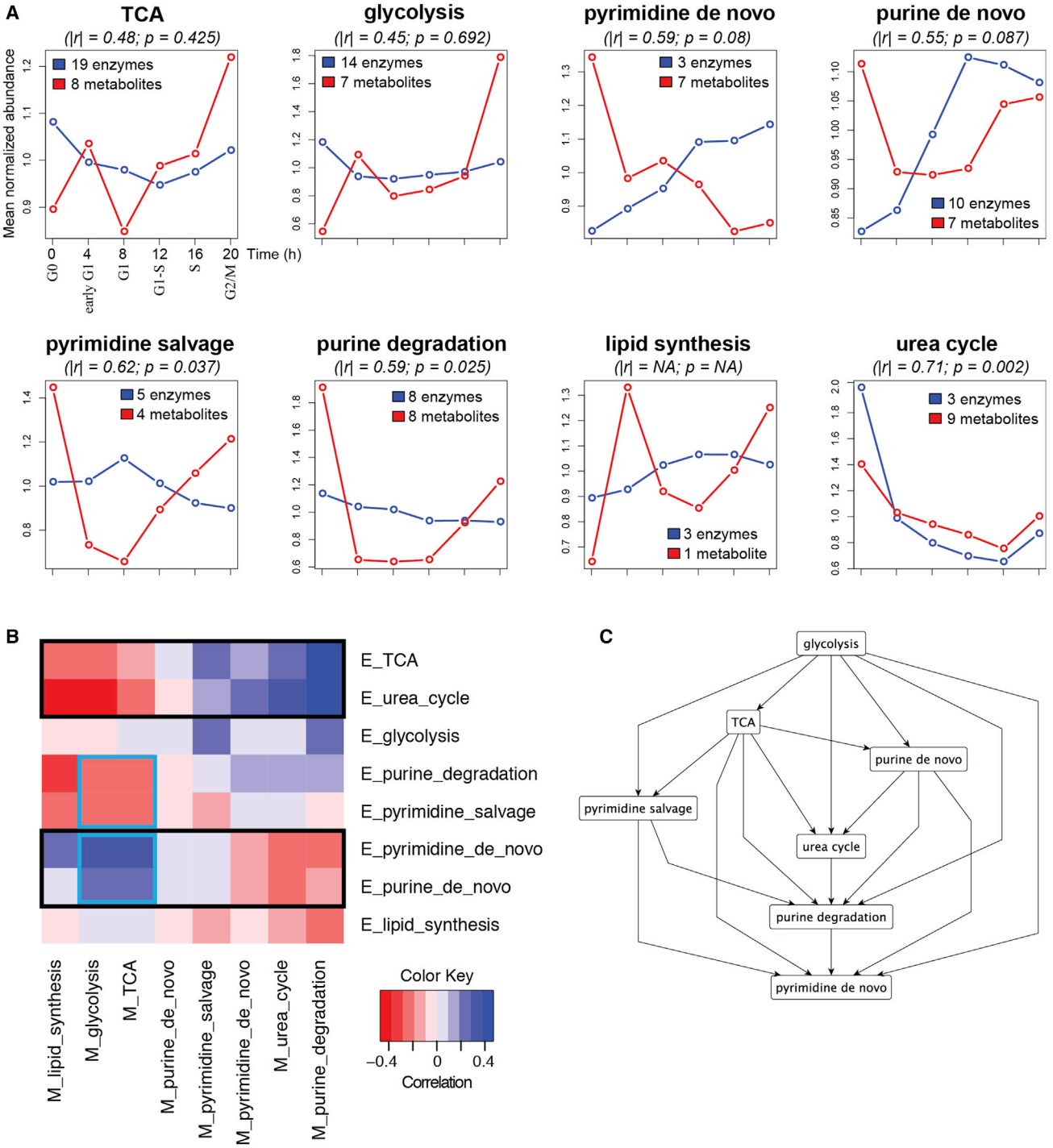

Figure 5. Correlation between Enzymes and Metabolites for Each Pathway and Cross-correlations among the Pathways

(A) Average abundance profiles of all enzymes and metabolites for eight pathways detected in our experiments. Enzyme profiles are indicated in blue, and metabolite profiles are indicated in red. All abundance levels are normalized to their mean values over the 20 hr. The average values of absolute Pearson correlation coefficients between enzymes and metabolites (|r|) and p values (p) are also shown. NA, not available for lipid synthesis because it has only one metabolite measured (citrate).

(B) A heatmap of enzyme-metabolite cross-correlations. Notable correlation patterns are highlighted in the black and cyan boxes. E_ represents enzymes in rows, and M_ represents metabolites in columns.

(legend continued on next page)

formulation (Experimental Procedures; Figure S6A). The initial amino-acid concentrations vary significantly from as high as 1.15 mM (Arg) to 24.5 μM (Trp). Perhaps among the most interesting observations was the correlation between uptake and excretion among essential amino acids (EAAs) and non-essential amino acids (NEAAs; Figure 6B). Like alpha-ketoglutaric acid (αKG), Glu was released from cells (0.39 mM in G0 and 0.16–0.37 mM in the first cell cycle; Figure S6A), suggesting a large role for Gln in nucleotide biosynthesis and the release of Glu. Studies in cancer cell lines support this interpretation (Jain et al., 2012; Marin-Valencia et al., 2012). We also observed that the resting population (36 hr without IL-3) and the proliferating population in the late G1 phase (8 hr–12 hr) consumed amino acids to a similar degree.

Focusing on the nine measured EAAs, we calculated the difference in amino-acid consumption at two adjacent times to obtain the consumption rate in 4-hr intervals. In addition, we used the relative frequency of EAA abundance in proteins to normalize the uptake of a specific EAA to the rate of protein synthesis, assuming no other potential functions of these amino acids. For this purpose, we used the evolutionarily observed frequencies from a previous study (King and Jukes, 1969), which turns out to remain relatively constant, regardless of the biological context (Figure S6B). The normalized consumption plot revealed that Met (whose observed frequency in proteins is 1.8%) was consumed more than the other eight measured EAAs (whose average frequency in proteins is 4.9%) by about 2-fold during the late-G1 to S phase (8 hr–16 hr; Figures 6C and S6C–S6E). Met and the average of the other EAAs were consumed most during the late G1 and S phases (8h – 12h), the peak time when protein synthesis occurs. However, Met was consumed more at the G1-S phase (8 hr–12 hr) than at the G0-G1 phase (0 hr–4 hr) by about 12-fold, compared to 5.6-fold, on average, for the other amino acids. Met consumption becomes even higher than the other EAAs by about 4-fold if we exclude the conditional amino acid, Arg, whose consumption is highest at the early G1 phase (4 hr–8 hr; Figures S6D–S6E). The early response of Arg uptake to IL-3 activation is supported by the fact that the arginine metabolism is related to the downstream production of metabolites such as nitric oxide and polyamines that have an important role in cell growth and proliferation (Peranzoni et al., 2007; Satriano, 2004).

Met constitutes the primary metabolic input for S-adenosylmethionine (SAM) biosynthesis. SAM is the cofactor for methyl transfer reactions required to establish the epigenetic methyl marks on nascent DNA and histones (DNA and histone methylation) (Shyh-Chang et al., 2013; Varela-Rey et al., 2014). The peak consumption of Met (G1-S phase) closely tracks with the observed patterns in nucleotide biosynthesis, providing a rationale for both its relative increased rate of consumption and the cell-cycle position at which this occurs. Furthermore, a pathway analysis of metabolites with an MFC > 4 shows that two downstream metabolites, SAM and S-methyl-5-thioadenosine, exhibit intracellular abundance patterns that track 4 hr behind that of Met (Figure S6F). The importance of Met metabolism was also supported by the protein expression profile of Dnmt1, the major DNA methyltransferase for CpG cytosines to maintain the methylation pattern during replication (Figure 2D), which peaks during the S phase following high Met consumption during G1. There is also elevated expression of other Met-consuming epigenetic enzymes, including methionine synthase (Mtr) peaking at t = 12 hr (G1-S phase); SAM synthetase isoform type-2, Mat2a, peaking at t = 8 hr (mid-late G1 phase); lysine methyltransferase, Smyd2, peaking at t = 12 hr; and arginine methyltransferase, Prmt7, peaking at t = 12 hr, with MFCs between 1.4 and 3.8 (Figure 6D). Moreover, 1-methylnicotinamide (1MNA), which was recently reported to play a role as a methylation sink after obtaining the methyl group from SAM in the Met cycle in tumor cells (Ulanovskaya et al., 2013; Ye et al., 2017), is highly secreted in our system, with more than 16-fold increase in the media from t = 12 hr on (Figure 6D). The abundance of its precursor metabolite, nicotinamide, in the media is reduced as well as its intracellular abundance, as expected (Figure 6D). We further correlated Met consumption with the levels of five histone tri-methylation marks: H3K4me3, H3K9me3, K3K27me3, H3K36me3, and H3K79me3 (Figure 6E). The peaks of intracellular Met and SAM at 4 hr and 8 hr overlap with the peaks of the five tri-methylated histones at 12 hr, suggesting that Met was also consumed for histone methylation through SAM.

DISCUSSION

Our model system of FL5.12 cells in response to IL-3 is, perhaps, a superior model for the G0/G1 transition to the more common serum-starvation and refeeding experiments that carry with them the complexity of signals in serum and the concerns of synchronization and re-activation (Cooper and Gonzalez-Hernandez, 2009). While there still exists a significant fraction of cells that loses synchrony in our system along the cell cycle, a significant sub-population of cells remarkably gave rise to major known characteristics and features of each cell-cycle phase, as evidenced in Figures 1F and 2D. Therefore, our study improves a molecular understanding of cell cycle in a more quantitative way, despite potential limitations and caveats regarding intrinsically incomplete synchrony in our system such as difficult interpretations of metabolite abundance profiles discussed later.

Dynamicity of the functional protein modules registered unambiguously in our proteomic measurements. Enzyme abundance profiles revealed many aspects of cellular metabolism whose regulation by the cell cycle has previously not been as well appreciated. The metabolite profiling was more difficult to interpret. Whereas the proteomic data registers the enzyme levels, which would be expected to correlate with the flux through the pathways, steady-state metabolite concentrations can take

(C) The network diagram shows cross-correlation inter-relationships. The nodes represent pathways, and a link from pathway 1 to pathway 2 is established if enzymes in pathway 1 have higher correlations with metabolites in pathway 2 than with metabolites in pathway 1 itself, on average. We took absolute Pearson correlations for this network for simplicity. Using this representation scheme, we built a hierarchical structure of pathway relationships. Note that glycolysis is located at the top of the structure connecting to all the other pathways.
See also Table S2.

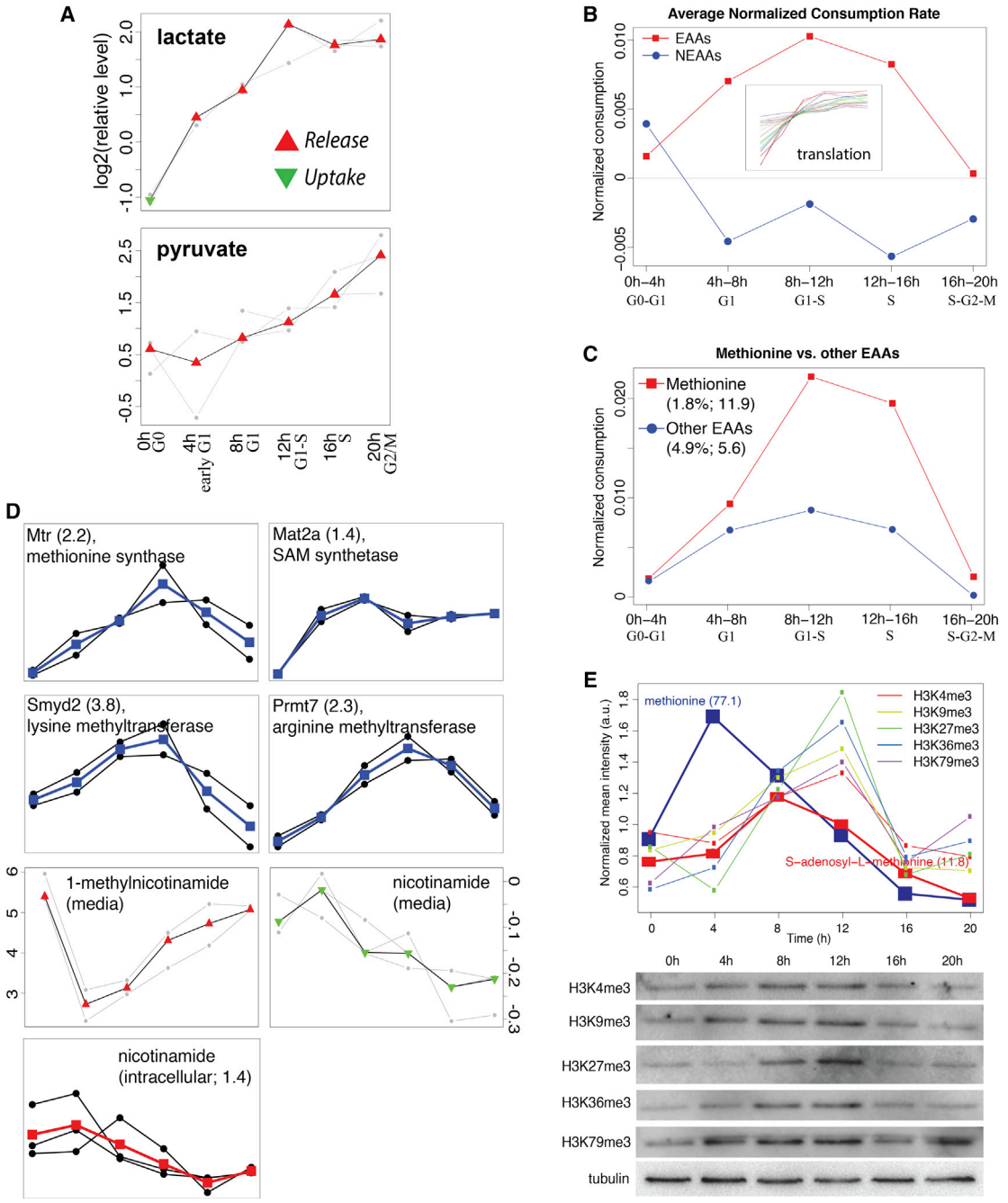

Figure 6. Media/Extracellular Metabolite Profiling and Methionine Metabolism

(A) Temporal profiles of lactate and pyruvate.

(B) Average normalized consumption rates of essential versus non-essential amino acids (EAAs versus NEAAs). The consumption of EAAs is correlated with upregulated protein profiles involved in translation.

(C) Normalized consumption rates of Met and the other eight essential amino acids. The numbers in the legend represents the relative frequency and the fold change of the consumption rates at 8 hr–12 hr and 0 hr–4 hr.

(D) Protein and metabolite profiles involved in Met metabolism.

(E) Intracellular levels of five histone tri-methylation marks were measured using western blot and quantified by normalizing to tubulin levels. The normalized levels were compared with intracellular abundance patterns of Met and SAM in an arbitrary scale for simplicity with MFC values in parentheses.

high or low values under conditions of high flux. For such reasons, steady-state metabolite levels are hard to relate to enzyme levels. In addition, numerous metabolites in central carbon metabolism can be substrates/products of multiple reactions in independent pathways, which can confuse any analysis based solely on the enzyme concentrations of the core pathways. Experimental measurement of flux using labeled substrates would help clarify these issues, as well as using better synchronized cell populations.

The changes of metabolic state in the G0-G1 transition in the pro-B lymphocyte line invite a comparison to cancer. Although there have been several studies of gene expression, proteomics, and metabolism in proliferation and quiescence (Coloff et al., 2016; Lemons et al., 2010; Valcourt et al., 2012; Venezia et al., 2004), a quantitative description of the proteome of G0 cells and their transition into the cell cycle has been generally lacking. Our proteomic survey shows that they are remarkably similar to recent studies of the G1 state in the cancer metabolism literature, where the cells are in a constant proliferative state (Muñoz-Pinedo et al., 2012; Schulze and Harris, 2012; Wheatley, 2005).

The metabolic profiling of extracellular metabolites revealed that Met consumption dramatically increases during the G1 phase compared to other EAAs. This would not be expected if all EAAs, including Met, were consumed only for protein synthesis. In that case, the amount of each EAA should reflect its relative abundance in the proteome. A similar observation was made for L-arginine in a recent proteomics and metabolomics study of activated human naive T cells (Geiger et al., 2016). An explanation for the high consumption of Met might be that it has additional functions, such as a source of methyl groups for protein methylation, including epigenetic marks (Waterland, 2006). Alternatively, highly proliferative cells could drain methyl groups from the Met cycle into 1MNA, decreasing histone/protein methylation (Ulanovskaya et al., 2013). Both appear to happen. We find that extracellular nicotinamide and 1MNA are anti-correlated with intracellular nicotinamide and 1MNA (Figure 6D), which could lead to a decrease of histone/protein methylation, despite higher Met intake. However, the proteomics data also support increased intracellular Met use. Mtr, an enzyme involved in Met synthesis, peaked at G1-S (Figure 6D), and the major DNA methyltransferase for replication, Dnmt1, as well as its interacting protein, Dmap1, for transcriptional repression, are upregulated during S phase (Rountree et al., 2000) (Figure 2D). These three upregulated proteins have each been investigated as therapeutic targets in cancer (Cheray et al., 2013; Tang et al., 2008). We also observed several other upregulated methyltransferases such as Dot1l, Prmt3/5/7, Smyd2, Ezh2, and Dnmt3b (Figures 6D and S7A). On the other hand, we observed diverse patterns of seven histone demethylases: Kdm1, Kdm3a, Kdm3b, Kdm4a, Kdm5b, Kdm5c, and Kdm6b (Figure S7B). Although we cannot attribute histone specificity of the individual methylating enzymes, the five histone trimethylation marks showed a temporal correlation with the levels of Met and SAM in their peak abundance levels (Figure 6E). A recent study also showed that histones could serve as a methylation sink (Ye et al., 2017), in addition to 1MNA. Moreover, the upregulation of Met and SAM from the mid-G1 phase is correlated with the downregulation of the two protein modules, SIRT1-LSD1 complex (MC289) and CtBP core complex (MC1067), which have roles in histone demethylation to repress target genes (DNA methylation in Figure S3B). We also note that homocysteine, a metabolite in the Met cycle, shows an opposite regulation pattern to Met and that the upregulation of homocysteine is accompanied by downregulation of glutathione peroxidase 1, Gpx1, a situation found in hyperhomocysteinemia (Figure S7C) (Handy et al., 2005). This suggests an additional demand for Met, which contributes to the interpretation of Met levels. The importance of Met and SAM for growth seems indisputable; a recent study reported that depletion of either Met or SAM induced G1 cell-cycle arrest in FL5.12 and its derivative cells (Lin et al., 2014).

The metabolomic and related proteomic map of IL-3 activation is summarized in Figure 7. It bears strong resemblance to features attributed to cancer cells. Based on our results outlined in this model, we suggest that IL-3-mediated activation of the cell cycle is similar to cancer in several important ways as follows and sheds light on cancer metabolism. Modules and proteins that are highly abundant in G0 are then abundant again from the S phase onward (Figure 7A, purple and blue bars, indicating "modules" and "proteins," respectively). These changes offer clues about how cancer cells may adapt in nutrient-deprived states (G0) and how they progress after tumorigenic transformation (S phase onward). Dynamic changes in intracellular metabolite levels are evident in G0, early G1, S, and G2/M phases (MFC > 2.49; Figure 7A, yellow bars, "intra"). These results suggest that metabolic activity is most evident during these stages of the cell cycle. These cells are the most avid for extracellular nutrients (i.e., uptake) in early G1, S, and G2/M phases (Figure 7A, green bars, "extra in"). On the other hand, metabolite release occurs mostly in G0 and G2/M phases (Figure 7A, red bars, "extra out"). These results parallel the catabolic (nutrient breakdown for energy) versus anabolic (nutrient capture for biosynthesis) phases of the cell cycle. Based on this, we can hypothesize a potential relationship between our model and cancer studies: cancer adaptation occurs in G0 (e.g., Eef2k and Eif4e3), oncogenic transformation in G0/G1 (e.g., Nek6 and Phlda1), and cancer progression during the first cell cycle (e.g., Rrm2). Among cancer types, our study will be immediately relevant as a tool to understand underlying molecular mechanisms of acute myeloid leukemias (AMLs), which possess abnormalities of the IL-3 receptor alpha chain, IL-3Ra, or CD123 (Muñoz et al., 2001; Steelman et al., 2004; Testa et al., 2004, 2014).

A major question in the field of cancer metabolism concerns how to target metabolic features of cancer cells that are often shared with normal proliferative and/or stem cells (Vander Heiden, 2011). Given that many of the metabolic characteristics of the proliferative transition in our system are seen in cancers, our findings can be explored carefully for therapeutic windows based on cancer metabolism. Furthermore, we also expect that our system provides insight into cancer metabolism directly and how its dysregulation can be used to select metabolic enzyme targets, pathways, and networks (Zhao et al., 2013). In particular, nucleotide-metabolism-targeted chemotherapies

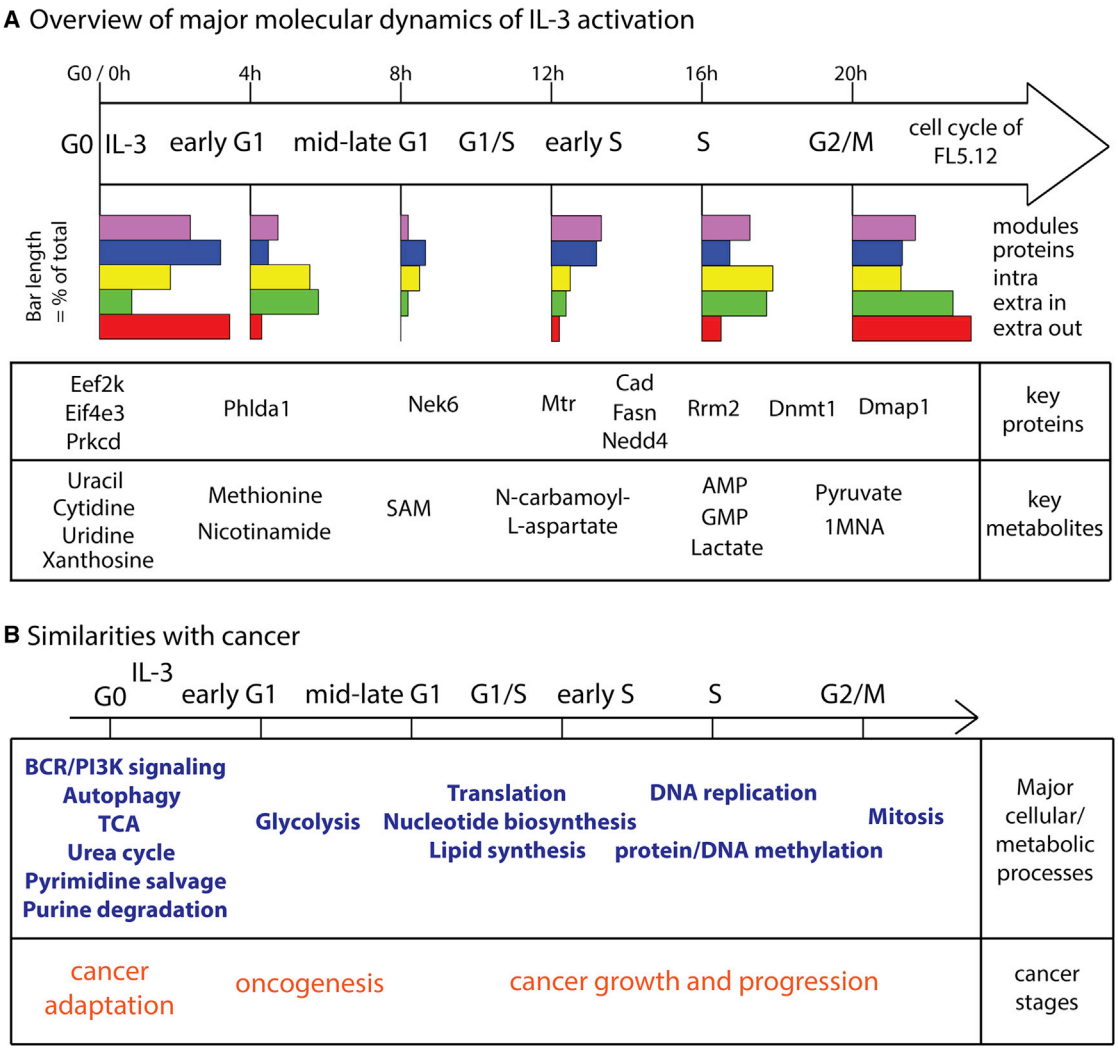

Figure 7. A Model of IL-3 Activation of FL5.12 Cells and a Relationship to Cancer Studies

(A) An overview of molecular dynamics from our proteomics and metabolomics data of IL-3 activation in terms of five classes of the most abundant molecules across the cell-cycle phases. Each color bar at each time point represents a relative fraction (or percentage) of molecules in each class of the same color (100%) that have the maximal abundance at that time point, showing temporal distributions of the most abundant molecular fractions in each class. We only selected those molecules in each class with MFCs that were greater than their median values, i.e., the top 50%. The five classes are: protein complexes/modules in purple ("modules"), individual proteins in blue ("proteins"), intracellular metabolites in yellow ("intra"), uptaken extracellular metabolites in green ("extra in"), and released extracellular metabolites in red ("extra out"). The median MFCs of the five classes are 1.24, 1.37, 2.49, 1.3, and 1.66, respectively. Several key proteins and metabolites with maximal abundance at each time point are shown in the table.

(B) Our model with major cellular and metabolic processes most affected or active across the cell-cycle phases showing similarities with the typical cancer stages.

have high associated toxicities, because this is a feature shared with normal proliferative cells.

EXPERIMENTAL PROCEDURES

Experimental Model

A murine pro-B lymphocyte cell line, FL5.12-Bcl-2, was a gift from Dr. Anthony Letai at the Dana Farber Cancer Institute. The cells were cultured in RPMI 1640 (Invitrogen) supplemented with 10% calf bovine serum (ATCC, catalog #30-2030), 1% 100× penicillin/streptomycin (Gemini), 1% Geneticin (Invitrogen, catalog #10131-035), and 50 mM 2-mercaptoethanol (Sigma/Aldrich), and 3 ng/mL IL-3 (R&D Systems, catalog #403-ML-010). For the G0 synchronization, the cycling cells were washed three times with warm PBS and then cultured in the same media, excluding IL-3, for 36 hr. For activation, the quiescent cells were re-suspended in the complete media including IL-3.

Cellular and Molecular Assays

Cell number counting, cell size measurement, AO assay, BrdU assay, and western blotting are described in the Supplemental Experimental Procedures.

TMT-MS Proteomics

For details, see the Supplemental Experimental Procedures.

Liquid Chromatography-Tandem MS Targeted MS Metabolomics

For details, see the Supplemental Experimental Procedures.

Bioinformatic and Statistical Analysis

Quantification of abundance levels of proteomics, metabolomics, and protein modules is detailed in the Supplemental Experimental Procedures. In general, p values less than 0.05 were considered significant.

Data and Software Availability

The proteomics, metabolomics, and protein modules profiling data processed in this study are available in the spreadsheet file with this article online (Data S1). All software is freely available and listed in the Resource Table in the Supplemental Experimental Procedures.

ACCESSION NUMBERS

The accession number for the proteomics dataset reported in this study is Proteome Xchange: PXD006771 (http://proteomecentral.proteomexchange.org/cgi/GetDataset?ID=PXD006771).

SUPPLEMENTAL INFORMATION

Supplemental Information includes Supplemental Experimental Procedures, seven figures, two tables, and one data file and can be found with this article online at http://dx.doi.org/10.1016/j.celrep.2017.06.074.

AUTHOR CONTRIBUTIONS

H.-J.L., M.P.J., S.P.G., L.C.C., and M.W.K. performed proteomics experiments and data analysis and interpretation. H.-J.L., C.A.L., J.M.A., L.C.C., and M.W.K. performed metabolomics experiments and data analysis and interpretation. H.-J.L., A.V., Y.H., N.P., and M.W.K. performed protein module analysis and data interpretation. H.-J.L. and J.K.M. performed flow cytometry. H.-J.L., N.W., N.S.-C., and C.M.-W. performed western blotting. H.-J.L., M.P.J., C.A.L., A.V., and M.W.K. wrote the paper.

ACKNOWLEDGMENTS

We would like to thank the M.W.K. lab members, Tim Mitchison, Joseph Loscalzo, Selina Chen-Kian, Zoltan Maliga, and an anonymous reviewer for their valuable comments and suggestions. This work was supported by National Institute of General Medical Sciences grant #GM26985 to M.W.K. and NIH grant #R01 GM041890 to L.C.C. L.C.C. owns equity in, receives compensation from, and serves on the Board of Directors and the Scientific Advisory Board of Agios Pharmaceuticals. Agios Pharmaceuticals is identifying metabolic pathways of cancer cells and developing drugs to inhibit such enzymes to disrupt tumor cell growth and survival.

Received: March 20, 2017
Revised: May 22, 2017
Accepted: June 25, 2017
Published: July 18, 2017

REFERENCES

Bauer, D.E., Harris, M.H., Plas, D.R., Lum, J.J., Hammerman, P.S., Rathmell, J.C., Riley, J.L., and Thompson, C.B. (2004). Cytokine stimulation of aerobic glycolysis in hematopoietic cells exceeds proliferative demand. FASEB J. *18*, 1303–1305.

Cheray, M., Pacaud, R., Nadaradjane, A., Vallette, F.M., and Cartron, P.F. (2013). Specific inhibition of one DNMT1-including complex influences tumor initiation and progression. Clin. Epigenetics *5*, 9.

Coloff, J.L., Murphy, J.P., Braun, C.R., Harris, I.S., Shelton, L.M., Kami, K., Gygi, S.P., Selfors, L.M., and Brugge, J.S. (2016). Differential glutamate metabolism in proliferating and quiescent mammary epithelial cells. Cell Metab. *23*, 867–880.

Conlon, I., and Raff, M. (1999). Size control in animal development. Cell *96*, 235–244.

Cooper, S., and Gonzalez-Hernandez, M. (2009). Experimental reconsideration of the utility of serum starvation as a method for synchronizing mammalian cells. Cell Biol. Int. *33*, 71–77.

Feun, L., You, M., Wu, C.J., Kuo, M.T., Wangpaichitr, M., Spector, S., and Savaraj, N. (2008). Arginine deprivation as a targeted therapy for cancer. Curr. Pharm. Des. *14*, 1049–1057.

Geiger, R., Rieckmann, J.C., Wolf, T., Basso, C., Feng, Y., Fuhrer, T., Kogadeeva, M., Picotti, P., Meissner, F., Mann, M., et al. (2016). L-arginine modulates T cell metabolism and enhances survival and anti-tumor activity. Cell *167*, 829–842.e13.

Handy, D.E., Zhang, Y., and Loscalzo, J. (2005). Homocysteine down-regulates cellular glutathione peroxidase (GPx1) by decreasing translation. J. Biol. Chem. *280*, 15518–15525.

Hirschler-Laszkiewicz, I., Cavanaugh, A.H., Mirza, A., Lun, M., Hu, Q., Smink, T., and Rothblum, L.I. (2003). Rrn3 becomes inactivated in the process of ribosomal DNA transcription. J. Biol. Chem. *278*, 18953–18959.

Jain, M., Nilsson, R., Sharma, S., Madhusudhan, N., Kitami, T., Souza, A.L., Kafri, R., Kirschner, M.W., Clish, C.B., and Mootha, V.K. (2012). Metabolite profiling identifies a key role for glycine in rapid cancer cell proliferation. Science *336*, 1040–1044.

Jeon, Y.J., Lee, K.Y., Cho, Y.Y., Pugliese, A., Kim, H.G., Jeong, C.H., Bode, A.M., and Dong, Z. (2010). Role of NEK6 in tumor promoter-induced transformation in JB6 C141 mouse skin epidermal cells. J. Biol. Chem. *285*, 28126–28133.

King, J.L., and Jukes, T.H. (1969). Non-Darwinian evolution. Science *164*, 788–798.

Lemons, J.M., Feng, X.J., Bennett, B.D., Legesse-Miller, A., Johnson, E.L., Raitman, I., Pollina, E.A., Rabitz, H.A., Rabinowitz, J.D., and Coller, H.A. (2010). Quiescent fibroblasts exhibit high metabolic activity. PLoS Biol. *8*, e1000514.

Levi, L., Lobo, G., Doud, M.K., von Lintig, J., Seachrist, D., Tochtrop, G.P., and Noy, N. (2013). Genetic ablation of the fatty acid-binding protein FABP5 suppresses HER2-induced mammary tumorigenesis. Cancer Res. *73*, 4770–4780.

Lin, D.W., Chung, B.P., and Kaiser, P. (2014). S-adenosylmethionine limitation induces p38 mitogen-activated protein kinase and triggers cell cycle arrest in G1. J. Cell Sci. *127*, 50–59.

Liu, R.Z., Graham, K., Glubrecht, D.D., Germain, D.R., Mackey, J.R., and Godbout, R. (2011). Association of FABP5 expression with poor survival in triple-negative breast cancer: implication for retinoic acid therapy. Am. J. Pathol. *178*, 997–1008.

London, L., and McKearn, J.P. (1987). Activation and growth of colony-stimulating factor-dependent cell lines is cell cycle stage dependent. J. Exp. Med. *166*, 1419–1435.

Malumbres, M., and Barbacid, M. (2005). Mammalian cyclin-dependent kinases. Trends Biochem. Sci. *30*, 630–641.

Marin-Valencia, I., Yang, C., Mashimo, T., Cho, S., Baek, H., Yang, X.L., Rajagopalan, K.N., Maddie, M., Vemireddy, V., Zhao, Z., et al. (2012). Analysis of tumor metabolism reveals mitochondrial glucose oxidation in genetically diverse human glioblastomas in the mouse brain in vivo. Cell Metab. *15*, 827–837.

McKearn, J.P., McCubrey, J., and Fagg, B. (1985). Enrichment of hematopoietic precursor cells and cloning of multipotential B-lymphocyte precursors. Proc. Natl. Acad. Sci. USA *82*, 7414–7418.

Meirelles, G.V., Perez, A.M., de Souza, E.E., Basei, F.L., Papa, P.F., Melo Hanchuk, T.D., Cardoso, V.B., and Kobarg, J. (2014). "Stop Ne(c)king around": How interactomics contributes to functionally characterize Nek family kinases. World J. Biol. Chem. *5*, 141–160.

Morris, S.M., Jr. (2002). Regulation of enzymes of the urea cycle and arginine metabolism. Annu. Rev. Nutr. *22*, 87–105.

Muñoz, L., Nomdedéu, J.F., López, O., Carnicer, M.J., Bellido, M., Aventín, A., Brunet, S., and Sierra, J. (2001). Interleukin-3 receptor alpha chain (CD123) is widely expressed in hematologic malignancies. Haematologica *86*, 1261–1269.

Muñoz-Pinedo, C., El Mjiyad, N., and Ricci, J.E. (2012). Cancer metabolism: current perspectives and future directions. Cell Death Dis. *3*, e248.

Murray, A.W. (2004). Recycling the cell cycle: cyclins revisited. Cell *116*, 221–234.

Nassirpour, R., Shao, L., Flanagan, P., Abrams, T., Jallal, B., Smeal, T., and Yin, M.J. (2010). Nek6 mediates human cancer cell transformation and is a potential cancer therapeutic target. Mol. Cancer Res. *8*, 717–728.

Nuñez, G., London, L., Hockenbery, D., Alexander, M., McKearn, J.P., and Korsmeyer, S.J. (1990). Deregulated Bcl-2 gene expression selectively prolongs survival of growth factor-deprived hemopoietic cell lines. J. Immunol. *144*, 3602–3610.

Orr, S.J., Boutz, D.R., Wang, R., Chronis, C., Lea, N.C., Thayaparan, T., Hamilton, E., Milewicz, H., Blanc, E., Mufti, G.J., et al. (2012). Proteomic and protein interaction network analysis of human T lymphocytes during cell-cycle entry. Mol. Syst. Biol. *8*, 573.

Pardee, A.B. (1989). G1 events and regulation of cell proliferation. Science *246*, 603–608.

Park, C.G., Lee, S.Y., Kandala, G., Lee, S.Y., and Choi, Y. (1996). A novel gene product that couples TCR signaling to Fas(CD95) expression in activation-induced cell death. Immunity *4*, 583–591.

Peranzoni, E., Marigo, I., Dolcetti, L., Ugel, S., Sonda, N., Taschin, E., Mantelli, B., Bronte, V., and Zanovello, P. (2007). Role of arginine metabolism in immunity and immunopathology. Immunobiology *212*, 795–812.

Peters, S.J. (2003). Regulation of PDH activity and isoform expression: diet and exercise. Biochem. Soc. Trans. *31*, 1274–1280.

Phillips, M.M., Sheaff, M.T., and Szlosarek, P.W. (2013). Targeting arginine-dependent cancers with arginine-degrading enzymes: opportunities and challenges. Cancer Res. Treat. *45*, 251–262.

Planas-Silva, M.D., and Weinberg, R.A. (1997). The restriction point and control of cell proliferation. Curr. Opin. Cell Biol. *9*, 768–772.

Ron-Harel, N., Santos, D., Ghergurovich, J.M., Sage, P.T., Reddy, A., Lovitch, S.B., Dephoure, N., Satterstrom, F.K., Sheffer, M., Spinelli, J.B., et al. (2016). Mitochondrial biogenesis and proteome remodeling promote one-carbon metabolism for T cell activation. Cell Metab. *24*, 104–117.

Rountree, M.R., Bachman, K.E., and Baylin, S.B. (2000). DNMT1 binds HDAC2 and a new co-repressor, DMAP1, to form a complex at replication foci. Nat. Genet. *25*, 269–277.

Satriano, J. (2004). Arginine pathways and the inflammatory response: interregulation of nitric oxide and polyamines: review article. Amino Acids *26*, 321–329.

Schulze, A., and Harris, A.L. (2012). How cancer metabolism is tuned for proliferation and vulnerable to disruption. Nature *491*, 364–373.

Shalev, I., Liu, H., Koscik, C., Bartczak, A., Javadi, M., Wong, K.M., Maknojia, A., He, W., Liu, M.F., Diao, J., et al. (2008). Targeted deletion of fgl2 leads to impaired regulatory T cell activity and development of autoimmune glomerulonephritis. J. Immunol. *180*, 249–260.

Sherr, C.J. (1994). G1 phase progression: cycling on cue. Cell *79*, 551–555.

Sherr, C.J., and Roberts, J.M. (2004). Living with or without cyclins and cyclin-dependent kinases. Genes Dev. *18*, 2699–2711.

Shyh-Chang, N., Locasale, J.W., Lyssiotis, C.A., Zheng, Y., Teo, R.Y., Ratanasirintrawoot, S., Zhang, J., Onder, T., Unternaehrer, J.J., Zhu, H., et al. (2013). Influence of threonine metabolism on S-adenosylmethionine and histone methylation. Science *339*, 222–226.

Singh, S.A., Winter, D., Kirchner, M., Chauhan, R., Ahmed, S., Ozlu, N., Tzur, A., Steen, J.A., and Steen, H. (2014). Co-regulation proteomics reveals substrates and mechanisms of APC/C-dependent degradation. EMBO J. *33*, 385–399.

Steelman, L.S., Pohnert, S.C., Shelton, J.G., Franklin, R.A., Bertrand, F.E., and McCubrey, J.A. (2004). JAK/STAT, Raf/MEK/ERK, PI3K/Akt and BCR-ABL in cell cycle progression and leukemogenesis. Leukemia *18*, 189–218.

Tang, C., Zhang, Z., Xu, B., Li, M., Liu, J., and Cui, J. (2008). Two newly synthesized 5-methyltetrahydrofolate-like compounds inhibit methionine synthase activity accompanied by cell cycle arrest in G1/S phase and apoptosis in vitro. Anticancer Drugs *19*, 697–704.

Testa, U., Riccioni, R., Diverio, D., Rossini, A., Lo Coco, F., and Peschle, C. (2004). Interleukin-3 receptor in acute leukemia. Leukemia *18*, 219–226.

Testa, U., Pelosi, E., and Frankel, A. (2014). CD 123 is a membrane biomarker and a therapeutic target in hematologic malignancies. Biomark. Res. *2*, 4.

Thompson, A., Schäfer, J., Kuhn, K., Kienle, S., Schwarz, J., Schmidt, G., Neumann, T., Johnstone, R., Mohammed, A.K., and Hamon, C. (2003). Tandem mass tags: a novel quantification strategy for comparative analysis of complex protein mixtures by MS/MS. Anal. Chem. *75*, 1895–1904.

Ting, L., Rad, R., Gygi, S.P., and Haas, W. (2011). MS3 eliminates ratio distortion in isobaric multiplexed quantitative proteomics. Nat. Methods *8*, 937–940.

Toyoshima, Y., Karas, M., Yakar, S., Dupont, J., Lee Helman, and LeRoith, D. (2004). TDAG51 mediates the effects of insulin-like growth factor I (IGF-I) on cell survival. J. Biol. Chem. *279*, 25898–25904.

Ulanovskaya, O.A., Zuhl, A.M., and Cravatt, B.F. (2013). NNMT promotes epigenetic remodeling in cancer by creating a metabolic methylation sink. Nat. Chem. Biol. *9*, 300–306.

Valcourt, J.R., Lemons, J.M., Haley, E.M., Kojima, M., Demuren, O.O., and Coller, H.A. (2012). Staying alive: metabolic adaptations to quiescence. Cell Cycle *11*, 1680–1696.

Vander Heiden, M.G. (2011). Targeting cancer metabolism: a therapeutic window opens. Nat. Rev. Drug Discov. *10*, 671–684.

Vander Heiden, M.G., Cantley, L.C., and Thompson, C.B. (2009). Understanding the Warburg effect: the metabolic requirements of cell proliferation. Science *324*, 1029–1033.

Varela-Rey, M., Iruarrizaga-Lejarreta, M., Lozano, J.J., Aransay, A.M., Fernandez, A.F., Lavin, J.L., Mósen-Ansorena, D., Berdasco, M., Turmaine, M., Luka, Z., et al. (2014). S-adenosylmethionine levels regulate the schwann cell DNA methylome. Neuron *81*, 1024–1039.

Venezia, T.A., Merchant, A.A., Ramos, C.A., Whitehouse, N.L., Young, A.S., Shaw, C.A., and Goodell, M.A. (2004). Molecular signatures of proliferation and quiescence in hematopoietic stem cells. PLoS Biol. *2*, e301.

Vinayagam, A., Hu, Y., Kulkarni, M., Roesel, C., Sopko, R., Mohr, S.E., and Perrimon, N. (2013). Protein complex-based analysis framework for high-throughput data sets. Sci. Signal. *6*, rs5.

Ward, P.S., and Thompson, C.B. (2012). Metabolic reprogramming: a cancer hallmark even warburg did not anticipate. Cancer Cell *21*, 297–308.

Waterland, R.A. (2006). Assessing the effects of high methionine intake on DNA methylation. J. Nutr. *136* (*6, Suppl*), 1706S–1710S.

Wheatley, D.N. (2005). Arginine deprivation and metabolomics: important aspects of intermediary metabolism in relation to the differential sensitivity of normal and tumour cells. Semin. Cancer Biol. *15*, 247–253.

Wu, N., Zheng, B., Shaywitz, A., Dagon, Y., Tower, C., Bellinger, G., Shen, C.H., Wen, J., Asara, J., McGraw, T.E., et al. (2013). AMPK-dependent degradation of TXNIP upon energy stress leads to enhanced glucose uptake via GLUT1. Mol. Cell *49*, 1167–1175.

Ye, C., Sutter, B.M., Wang, Y., Kuang, Z., and Tu, B.P. (2017). A metabolic function for phospholipid and histone methylation. Mol. Cell *66*, 180–193.e8.

Ying, H., Kimmelman, A.C., Lyssiotis, C.A., Hua, S., Chu, G.C., Fletcher-Sananikone, E., Locasale, J.W., Son, J., Zhang, H., Coloff, J.L., et al. (2012). Oncogenic Kras maintains pancreatic tumors through regulation of anabolic glucose metabolism. Cell *149*, 656–670.

Yuan, M., Breitkopf, S.B., Yang, X., and Asara, J.M. (2012). A positive/negative ion-switching, targeted mass spectrometry-based metabolomics platform for bodily fluids, cells, and fresh and fixed tissue. Nat. Protoc. *7*, 872–881.

Yun, J., Rago, C., Cheong, I., Pagliarini, R., Angenendt, P., Rajagopalan, H., Schmidt, K., Willson, J.K., Markowitz, S., Zhou, S., et al. (2009). Glucose deprivation contributes to the development of KRAS pathway mutations in tumor cells. Science *325*, 1555–1559.

Zetterberg, A. (1990). Control of mammalian cell proliferation. Curr. Opin. Cell Biol. *2*, 296–300.

Zetterberg, A., Larsson, O., and Wiman, K.G. (1995). What is the restriction point? Curr. Opin. Cell Biol. *7*, 835–842.

Zhao, Y., Butler, E.B., and Tan, M. (2013). Targeting cellular metabolism to improve cancer therapeutics. Cell Death Dis. *4*, e532.